Available online at www.sciencedirect.com
ScienceDirect
Journal of Organometallic Chemistry 692 (2007) 2253–2269
Journal of Organometallic Chemistry
www.elsevier.com/locate/jorganchem

Ditertiary phosphine derivatives of the heteronuclear cluster $RuOs_3(\mu\text{-}H)_2(CO)_{13}$

Yong Leng Kelvin Tan, Weng Kee Leong *

Department of Chemistry, National University of Singapore, Kent Ridge, Singapore 119260, Singapore

Received 17 January 2007; received in revised form 1 February 2007; accepted 1 February 2007
Available online 6 February 2007

Abstract

The heteronuclear cluster $RuOs_3(\mu\text{-}H)_2(CO)_{13}$ (**1**) reacted readily with a number of ditertiary phosphines under chemical activation with trimethylamine-*N*-oxide. The solid-state and solution structures of these derivatives have been examined. Six structural types have been characterized crystallographically, including one in which a phenyl group migrates from the ditertiary phosphine ligand to the metal framework. There are many more isomers present in solution, most of which are rapidly inter-converting via hydride migrations.

Keywords: Heterometallic; Ruthenium; Osmium; Ditertiary phosphines; Isomers

1. Introduction

Heteronuclear clusters containing group homologues are of interest as the different transition metals present in close proximity can display subtle synergistic effects, giving rise to novel chemistry. One such family is the tetrahedral clusters with the formulae $M'M_3(\mu\text{-}H)_2(CO)_{13}$, where M and M′ are group 8 elements. Currently, three members of this family are known, viz., $FeRu_3(\mu\text{-}H)_2(CO)_{13}$, $FeOs_3(\mu\text{-}H)_2(CO)_{13}$, and $RuOs_3(\mu\text{-}H)_2(CO)_{13}$ (**1**). While the chemistry of $FeRu_3(\mu\text{-}H)_2(CO)_{13}$ and $FeOs_3(\mu\text{-}H)_2(CO)_{13}$ have been relatively well-investigated [1], the reactivity of **1** has been comparatively much less explored. It has been well-established that the chemistries of ruthenium and osmium are much more alike than they are to that of iron. We have recently reported a high-yield synthetic route to **1**, and have embarked on a series of investigations into its chemistry. The reactivity of **1** with group 15 ligands as well as various organic substrates has been described [2,3]. As part of our ongoing studies on the chemistry of **1** and its derivatives, we have examined the substitution chemistry of **1** with a number of representative ditertiary phosphines. We would like to report the results of this study here.

2. Results and discussion

The products from the reaction of **1** with a number of different ditertiary phosphines in the presence of 2 M equiv. of TMNO (trimethylamine-*N*-oxide) at ambient temperature are summarized in Scheme 1.

All these novel products have been characterized spectroscopically and analytically, and with the exception of **4f**, **8** and **9**, also by single-crystal X-ray crystallographic studies. The clusters will be grouped according to their structural types for the discussion that follows.

2.1. Ditertiary phosphine acting as an inter-cluster link

Clusters $[RuOs_3(\mu\text{-}H)_2(CO)_{10}(\mu\text{-}CO)_2]_2(\mu\text{-}L)$ (**2**) (L = dppe (**b**); dppp (**c**); dppb (**d**)) have the same general structure comprising two metal tetrahedra linked by a ditertiary phosphine ligand. The ORTEP plot showing the molecular structure of **2c**, which is representative, is given in Fig. 1. A common atomic numbering scheme, together with selected bond parameters for all three clusters are collected in Table 1.

* Corresponding author.
E-mail address: chmlwk@nus.edu.sg (W.K. Leong).

0022-328X/$ - see front matter © 2006 Elsevier B.V. All rights reserved.
doi:10.1016/j.jorganchem.2007.02.001

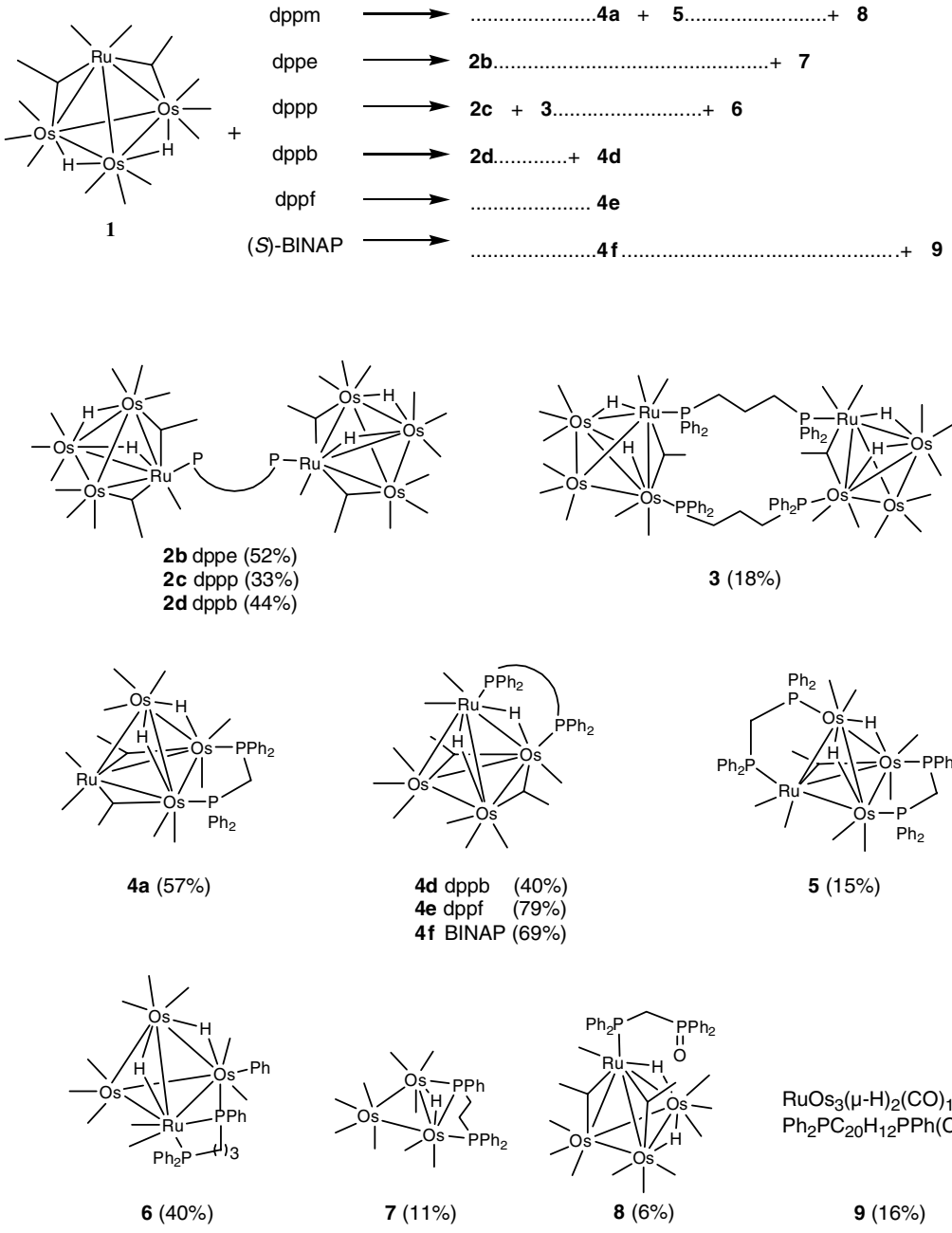

Scheme 1.

A comparison of the structural parameters indicates that they are similar to one another as well as to the monosubstituted ER_3 derivatives of **1** [2d]; this includes the relative dispositions of the hydrides and bridging carbonyls. As previously observed, there appears to be an electronic preference for substitution at an Ru vertex. Similarly, without exception, both hydrides in each metal tetrahedron share a common vertex. All the structures also exhibit bridging carbonyls, due to the greater electron density imparted to the cluster core by the strong σ donating phosphine ligand; bridging carbonyls are better π-acceptors than terminal CO ligands [4]. The crystals of **2b** and **2d** exhibited disorder of the metal framework. This disorder was equivalent to the presence of two isomers in a 1:1 and 4:1 ratio for **2b** and **2d**, respectively; the latter is similar to that observed for the PPh_3 derivative [2a]. For **2b**, this is in agreement with the observation of isomers in solution. The proposed solution state structures and tentative NMR assignments (phosphorus and hydride resonances) for **2b**–**d** have been made as shown in Fig. 2.

Besides **2c**, the reaction of **1** with dppp also yielded $[RuOs_3(\mu\text{-}H)_2(CO)_{10}(\mu\text{-}CO)]_2(\mu\text{-dppp})_2$ (**3**). A molecular plot of **3** is shown in Fig. 3, together with selected bond parameters. There was disorder of the metal framework, with ruthenium occupancies refined to 0.5:0.5 for M(1) and M(2), as well as for M(5) and M(6), respectively. In **3**, two tetrahedral metal cores are linked by the ditertiary phosphine ligand, resulting in a cyclic arrangement. The

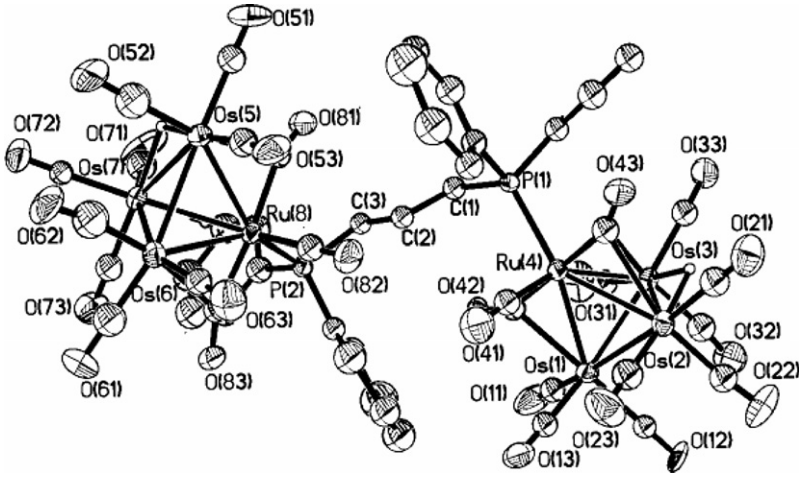

Fig. 1. ORTEP diagram (50% probability thermal ellipsoids, organic hydrogens omitted) for **2c**.

three bridging ligands lie on one triangular face of each tetrahedron. The NMR signals have been assigned with the aid of a $^{31}P\{^{1}H\}$–^{1}H HMBC spectrum as well as $^{1}H\{^{31}P\}$ selective decoupling experiments, and are depicted in Fig. 2. There are two sets of methylene resonances displayed in the organic region; selective decoupling experiments indicated that each set was coupled to only one of the two phosphorus resonances. For this reason we propose that each of the dppp ligands links vertices of the same atom type. Our attempts to obtain **3** by reacting **2c** with dppp proved unsuccessful. At this point in time, therefore, we have no clear rationalization as to how **3** could have been formed.

Table 1
Common atomic numbering scheme and selected bond parameters for **2b**–**2d**

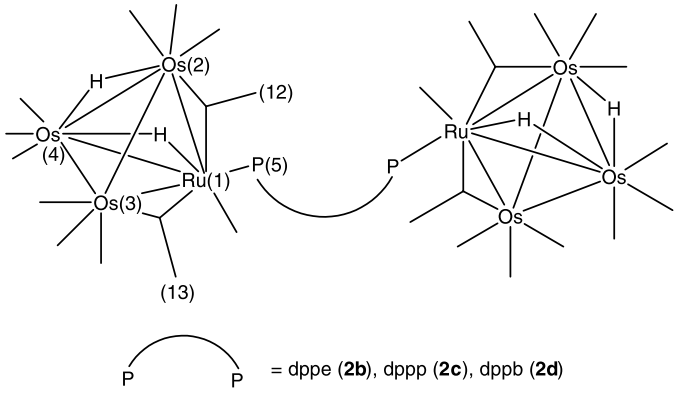

	2b	2c	2d
Bond lengths (Å)			
Ru(1)–Os(2)	2.8000(7)	2.800(2)	2.7972(5)
Ru(1)–Os(3)	2.7911(7)	2.790(2)	2.7806(5)
Ru(1)–Os(4)	2.9689(7)	2.959(2)	2.9660(5)
Os(2)–Os(3)	2.8433(7)	2.8464(14)	2.8470(4)
Os(2)–Os(4)	2.9374(6)	2.9325(14)	2.9325(4)
Os(3)–Os(4)	2.8011(6)	2.8038(14)	2.8035(4)
Ru(1)–P(5)	2.350(3)	2.369(6)	2.3653(17)
Ru(1)–C(12)	1.974(11)	1.96(3)	1.955(7)
Os(2)–C(12)	2.561(11)	2.52(3)	2.508(7)
Ru(1)–C(13)	1.989(10)	1.99(3)	1.993(7)
Os(3)–C(13)	2.381(11)	2.38(2)	2.406(8)
Bond angles (°)			
Ru(1)–C(12)–Os(2)	75.0(3)	76.4(8)	76.5(2)
Ru(1)–C(13)–Os(3)	78.8(4)	78.7(9)	77.8(3)

2.2. Ditertiary phosphine bridging a metal–metal bond

The major product of the reaction with dppm, dppb, dppf or (*S*)-BINAP was the clusters $RuOs_3(\mu\text{-}H)_2(CO)_9(\mu\text{-}CO)_2(\mu\text{-}L)$ (**4**) (L = dppm (**a**); dppb (**d**); dppf (**e**); (*S*)-BINAP (**f**)). The solid-state structures of **4a**, **4d** and **4e** have been established by single-crystal X-ray crystallographic studies. The structures of **4d** and **4e** are similar, while that for **4a** is an isomeric form. Suitable crystals of **4f** for X-ray crystal structural analysis could not be obtained despite several attempts. This is consistent with earlier observations that BINAP-substituted clusters are generally difficult to crystallize in a suitable form for X-ray crystallographic studies and the reported structures of such clusters are often not of ideal quality [5]. Nonetheless, the molecular structure of **4f** can be assigned with some certainty to be similar to those of **4d/e** by comparison of the infrared spectra. The ORTEP diagrams for **4a** and **4d** are displayed in Figs. 4 and 5, respectively. A common atomic numbering scheme and selected bond parameters for **4d** and **4e** are given in Table 2.

The crystals of all three compounds were found to exhibit disorder of the metal framework, which corresponded to the presence of two isomers in each case. The isomeric ratios were 0.76:0.24, 0.39:0.61 and 0.72:0.28 in **4a**, **4d** and **4e**, respectively. The clusters retained the tetrahedral metal framework of the parent cluster **1**, with the ditertiary phosphine ligand spanning one edge of the $RuOs_3$ tetrahedron. In **4d** and **4e**, the ditertiary phosphine ligands

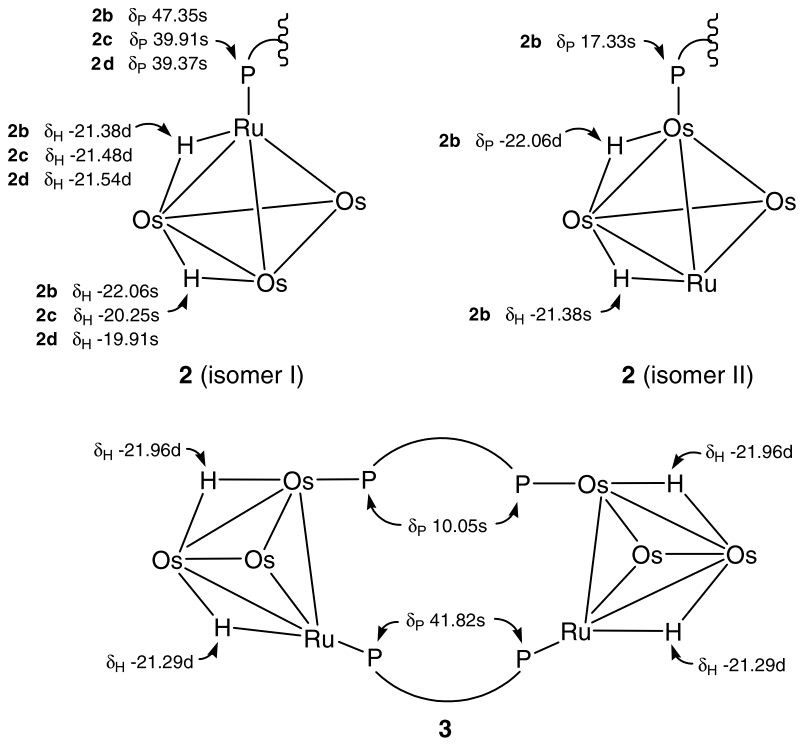

Fig. 2. Proposed solution state structures and tentative NMR (^{31}P and hydrides) assignments for **2b–d** and **3** (carbonyls omitted).

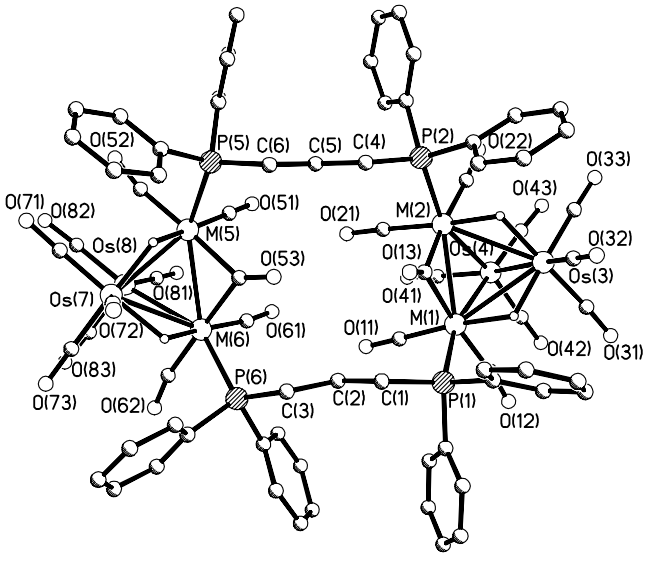

Fig. 3. Molecular plot and selected bond lengths (Å) and angles (°) for **3**: M(1)–M(2) = 2.7937(7); M(1)–Os(3) = 2.9516(6); M(1)–Os(4) = 2.8421(6); M(2)–Os(3) = 2.9547(6); M(2)–Os(4) = 2.8067(6); Os(3)–Os(4) = 2.7926(6); M(1)–P(1) = 2.361(2); M(2)–P(2) = 2.365(2); M(5)–M(6) = 2.7844(7); M(5)–Os(7) = 2.9575(7); M(5)–Os(8) = 2.8180(7); M(6)–Os(7) = 2.9585(6); M(6)–Os(8) = 2.8094(7); Os(7)–Os(8) = 2.7936(7); M(5)–P(5) = 2.371(3); M(6)–P(6) = 2.386(2); M(1)–C(13)–Os(2) = 82.2(3); M(5)–C(53)–M(6) = 82.1(4).

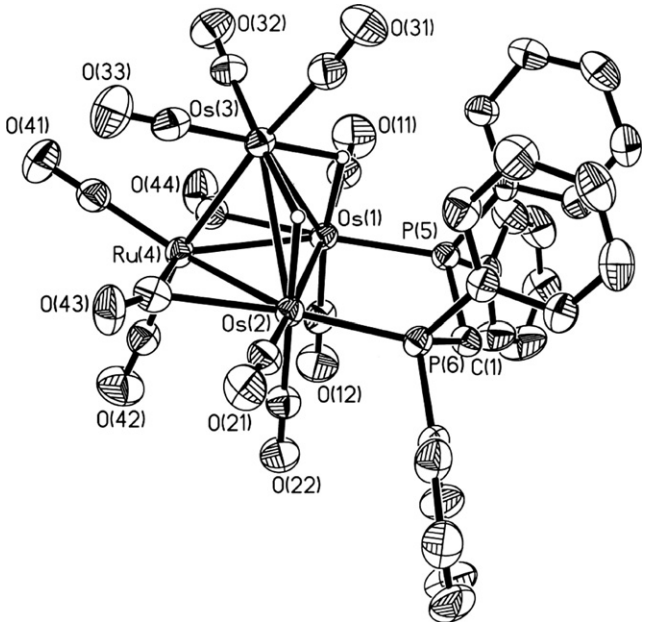

Fig. 4. ORTEP diagram (50% probability thermal ellipsoids, organic hydrogens omitted) and selected bond lengths (Å) and angles (°) for **4a**: Os(1)–Os(2) = 2.8580(3); Os(1)–Os(3) = 2.9688(4); Os(1)–Ru(4) = 2.8098(5); Os(2)–Os(3) = 3.0112(3); Os(2)–Ru(4) = 2.7871(4); Os(3)–Ru(4) = 2.7911(4); Os(1)–P(5) = 2.3189(15); Os(2)–P(6) = 2.3203(15); P(5)–Os(1)–Os(2) = 90.86(4); P(6)–Os(2)–Os(1) = 92.27(4); Ru(4)–C(44)–Os(1) = 79.6(2); Ru(4)–C(43)–Os(2) = 77.8(2). Disorder of ruthenium over Os(1), Os(2) and Ru(4) in 0.12:0.12:0.76 ratio.

spanned the hydride bridged Os(3)–Ru(4) bond; this edge is expected to be the most electron-rich site in the cluster [6]. There is an increase in both the metal–metal bond length as well as the M–M–P angles in order to accommodate the additional hydride and the steric requirements of the additional methylene (**4d**) or ferrocene (**4e**) groups [7]. In **4a**,

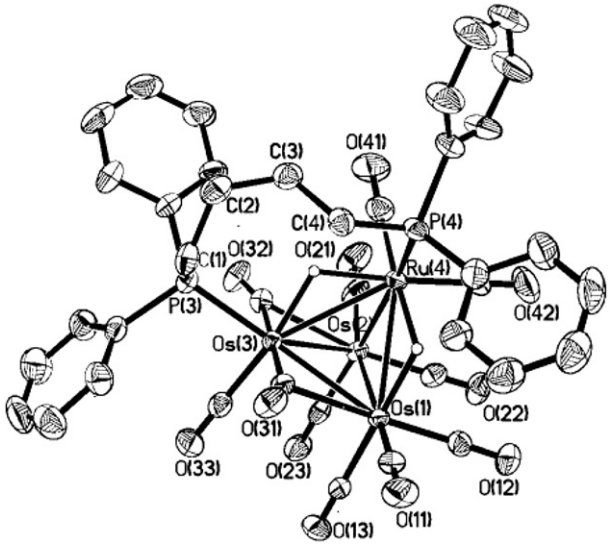

Fig. 5. ORTEP diagram (50% probability thermal ellipsoids, organic hydrogens omitted) for **4d**. There is disorder of the ruthenium over Os(3) and Ru(4) in a 0.39:0.61 ratio.

Table 2
Common atomic numbering scheme and selected bond parameters for **4d** and **4e**

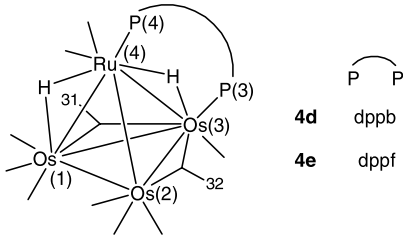

	4d	4e
Bond lengths (Å)		
Os(1)–Os(2)	2.8280(2)	2.8251(3)
Os(1)–Os(3)	2.8271(3)	2.8287(3)
Os(1)–Ru(4)	2.9452(3)	2.9522(4)
Os(2)–Os(3)	2.7901(3)	2.8093(3)
Os(2)–Ru(4)	2.7841(3)	2.7790(4)
Os(3)–Ru(4)	2.9577(3)	2.9799(4)
Os(3)–P(3)	2.3746(12)	2.3750(12)
Ru(4)–P(4)	2.3691(13)	2.3627(13)
Bond angles (°)		
P(3)–Os(3)–Ru(4)	114.98(3)	113.67(3)
P(4)–Ru(4)–Os(3)	109.79(3)	118.24(3)
Os(1)–C(31)–Os(3)	77.22(16)	78.65(19)
Os(2)–C(32)–Os(3)	76.99(16)	74.74(17)

neither of the two hydride ligands bridges the same metal–metal edge as the ditertiary phosphine ligand.

Consistent with the disorder found in the solid-state structures, the solution spectra of **4** pointed to the presence of more than one isomer in solution. In the tentative assignments of the solution structures, it was assumed that the various isomers could be attributed to different relative arrangements of the phosphorus and hydride ligands only, and that the carbonyl ligands were in rapid exchange. The latter was corroborated by the ambient temperature $^{13}C\{^1H\}$ NMR spectrum of **4d**, which showed no distinct CO resonances. The infrared spectra also showed broad (for **4a**), or no bridging carbonyl signals (for **4d**–**f**) although these groups were present in the solid-state structures, suggesting that CO exchange was fast even on the infrared timescale (10^{-11} s compared to $\sim10^{-5}$ s for NMR).

For **4a**, the NMR spectral measurements indicated the presence of two isomers in a 3:1 ratio, as reflected in the disorder in the solid-state structure. The solid-state structures may be assumed to persist in solution; the proposed solution state structures and tentative NMR assignments can be made as shown in Fig. 6. The assignments for the minor isomer of **4a** are consistent with earlier reports that the ^{31}P chemical shift for a phosphorus bonded to ruthenium is found at a lower field relative that for a phosphorus bonded to osmium [2,8], and the bridging hydride resonance in tetranuclear clusters is shifted increasingly upfield along the series Ru–Ru, Ru–Os and Os–Os [1].

Both the $^{31}P\{^1H\}$ and ^1H NMR spectra of **4d** also indicated the presence of two isomers in an ~3:1 ratio. The tentative structures and NMR assignments, elucidated with a $^{31}P\{^1H\}$–^1H HMBC and $^1H\{^{31}P\}$ selective decoupling experiments, are shown in Scheme 2. A ^1H EXSY spectrum taken at 300 K (Fig. 7) indicated chemical exchange between hydrides H_a and H_c, as well as between H_b and H_d, and NOE crosspeaks correlating H_a and H_b, as well as between H_c and H_d. The simplest intermolecular exchange pathway between the two isomers would entail the flipping of a hydride from an Ru–Os to an Os–Os edge (Scheme 2).

At ambient temperature the ^1H NMR and $^{31}P\{^1H\}$ NMR signals for **4e** are substantially broadened. On lowering the temperature, these resonances gradually sharpen and are resolved at 223 K, with eight sets of signals present in both the high-field region of the ^1H NMR (Fig. 8) as well as the $^{31}P\{^1H\}$ NMR spectra. These resonances have been ascribed to the presence of four isomers in solution; the P–P and P–H correlations have been determined through a $^{31}P\{^1H\}$–^1H HMBC acquired at 243 K (Fig. 9), while the coupling constants have been verified via $^1H\{^{31}P\}$ selective decoupling. We have tentatively assigned the structures in solution as corresponding to that implied by the disorder

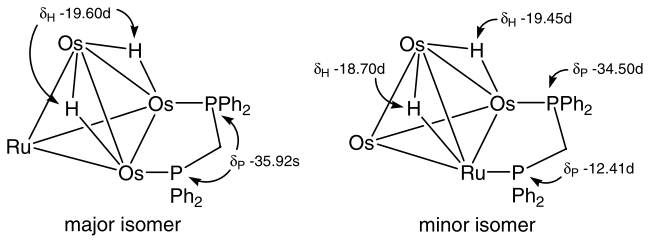

Fig. 6. Proposed solution state structures and tentative NMR assignments for**4a** (carbonyls omitted).

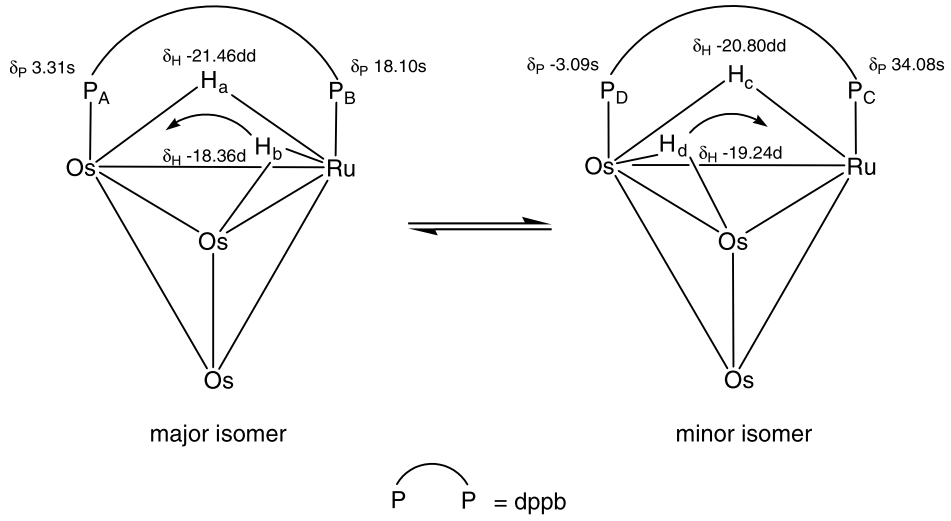

Scheme 2.

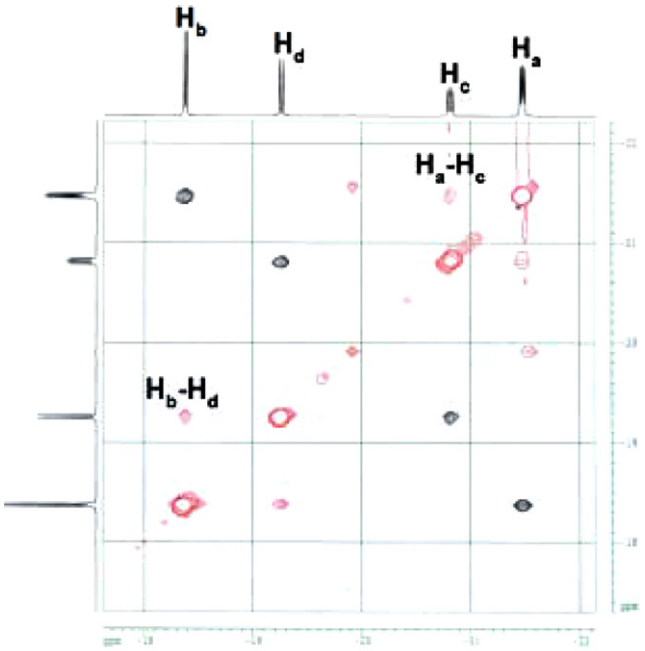

Fig. 7. ^{1}H EXSY spectrum (300 K) for **4d** ($\tau_m = 0.5$ s). Chemical exchange crosspeaks are labeled.

observed in the solid-state structure; these and the tentative NMR assignments are depicted in Scheme 3. The isomers differ in the position of one of the hydrides – whether it is bridging an Ru–Os edge (isomers I and II) or an Os–Os edge (isomers III and IV) – and in the conformation of the dppf. From NMR integration, the isomeric distribution obtained was 18:10:5:1 for isomers I:II:III:IV.

The dynamic behaviour of **4e** may be rationalized by a combination of three separate processes: (i) a conformational change in the dppf ligand, (ii) isomerization which involves flipping of a hydride ligand from an Ru–Os to an Os–Os edge, and (iii) mutual exchange of hydride positions within each isomer; the first two processes are also depicted in Scheme 3. The exchange crosspeaks from these processes are identifiable in a ^{1}H EXSY spectrum recorded at 243 K, and a reduction in the mixing time (from 0.5 to 0.1 s) gave exchange crosspeaks corresponding to process (i) above only, suggesting (as may be expected) that the conformational change of the dppf ligand occurs at a faster rate than hydride migration.

A similarly complex situation occurred for **4f**, in which there appeared to be seven isomeric species present in a 6.3:4.3:3.5:2.6:2.5:2.0:1.0 ratio. Tentative solution state structures for these isomers have been identified, and their NMR assignments made. The presence of the large number of isomers in solution is not unexpected as BINAP-containing clusters have been known to adopt different conformers which exchange rapidly in solution [9]. Although an EXSY spectrum could not be obtained due to the poor solubility of **4f** in CD_2Cl_2 at 183 K, it can be postulated that the isomers in **4f** should undergo similar exchange processes as proposed for **4e**, namely, conformational change of the BINAP ligand, hydride migration and intramolecular hydride exchange.

The reaction with dppm also afforded $RuOs_3(\mu\text{-}H)_2(CO)_8(\mu\text{-}CO)(\mu\text{-}dppm)_2$ (**5**) which comprised a metal tetrahedron with two of the metal–metal edges bridged by dppm ligands. An ORTEP plot of the molecular structure of **5** is shown in Fig. 10, together with selected structural parameters. The crystal of **5** exhibited disorder of the metal framework; this disorder was modeled with ruthenium over three alternative positions – M(4):M(2):M(1) – with ruthenium occupancies refined to about 0.7:0.2:0.1, respectively. No analogue of **5** has been reported for tetrahedral clusters of the iron subgroup. However examples from the cobalt subgroup are known, including $Rh_4(CO)_8(\mu\text{-}dppm)_2$ [10], $Co_4(CO)_8(\mu\text{-}dmpm)_2$ [11], and $Ir_4(CO)_8(\mu\text{-}dppm)_2$ [12]. Cluster **5** may be considered as having been derived from **4a** by replacement of two carbonyl groups by a second dppm ligand.

Cluster **5** was found to be relatively insoluble as well as unstable in solution, decomposing over time to give several

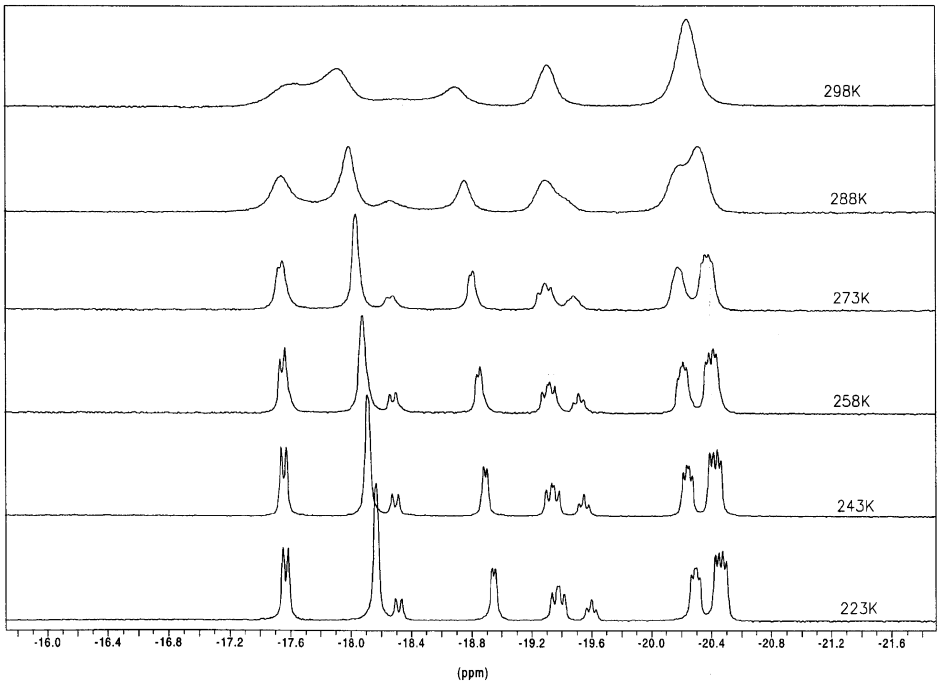

Fig. 8. Variable temperature ^{1}H NMR spectra (CD_2Cl_2, high field only) for **4e**.

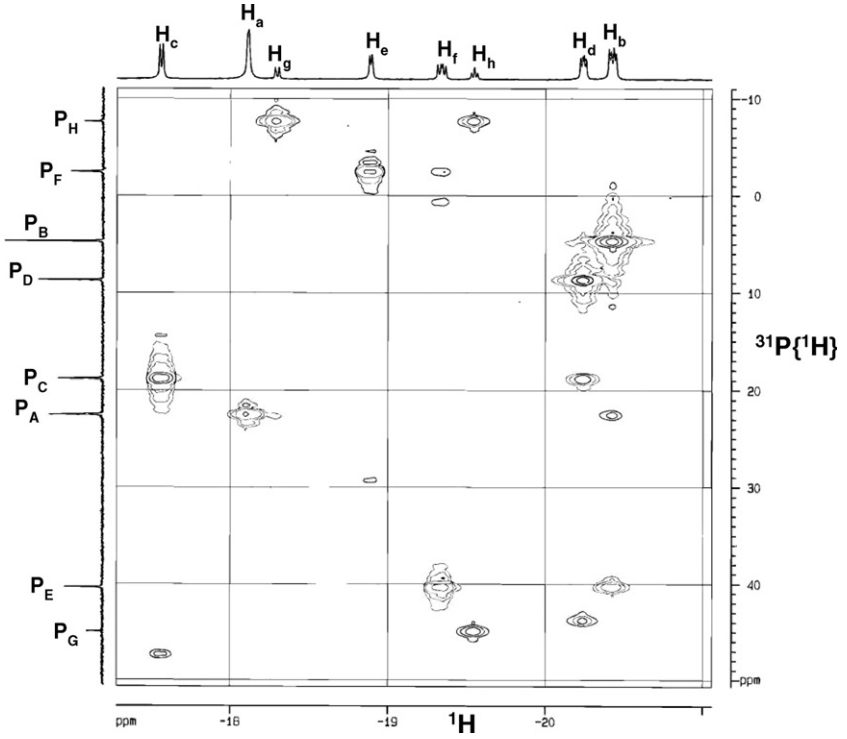

Fig. 9. $^{31}P\{^{1}H\}$–^{1}H HMBC spectrum (243 K) for **4e**.

unidentified products. The ^{1}H and $^{31}P\{^{1}H\}$ NMR spectra for **5** at ambient temperature in $CDCl_3$ were obtained with difficulty, and they indicated the presence of four isomers in an approximate 67:19:10:4 ratio. The proposed structures of these isomers are given in Fig. 11, together with the tentative NMR assignments for the two predominant isomers, which were made with the aid of ^{1}H–$^{31}P\{^{1}H\}$ HMBC, $^{31}P\{^{1}H\}$ and ^{1}H COSY, and $^{1}H\{^{31}P\}$ and $^{31}P\{^{31}P\}$ selective decoupling. The ^{31}P resonances for the two minor isomers (III and IV) were, unfortunately, not well resolved. Nonetheless, as the splitting patterns for each of the four sets of hydride resonances are similar, it is highly likely that isomers III and IV have structures similar to the isomers I and II in solution state, differing only in the

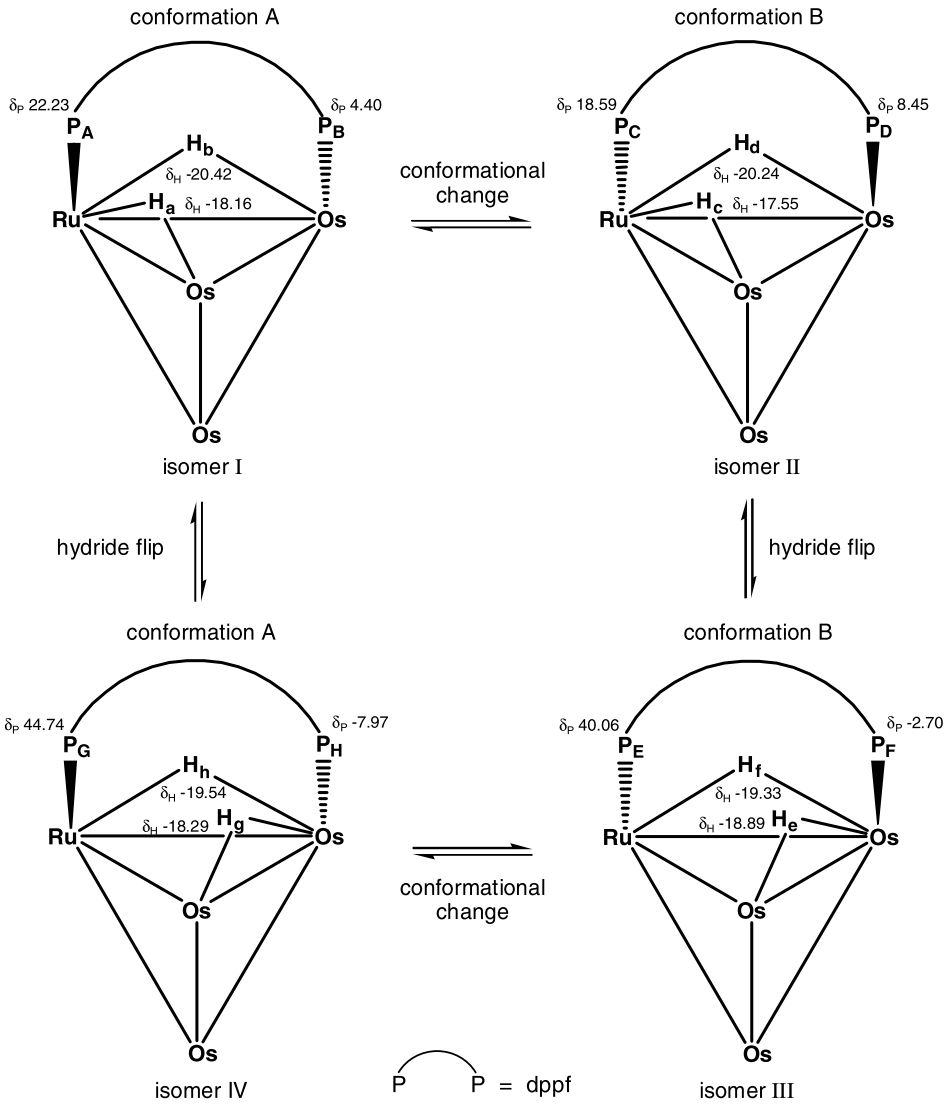

Scheme 3.

positions of the metal atoms. With the exception of IV, the proposed solution structures and their relative amounts are in excellent agreement with the disorder observed in the solid-state structure.

2.3. Phosphido ligand

The molecular structure of $RuOs_3(\mu\text{-}H)_2(CO)_{10}[\mu,\kappa^2{:}\kappa^1\text{-}PPh(CH_2)_3PPh_2](Ph)$ (**6**) is shown in Fig. 12, together with selected bond parameters. Cluster **6** may be regarded as derived from $RuOs_3(\mu\text{-}H)_2(CO)_{11}(\mu\text{-dppp})$ (**4c**) which was not isolated, via dephenylation. Ruthenium or osmium carbonyl clusters containing σ-bonded phenyl groups are rare; some examples include $Ru_3(\mu_3\text{-}PPhCH_2PPh_2)(\mu_3\text{-}C_8H_8)(Ph)(CO)_3$ [13], $Os_5(\mu_4\text{-}Sb)(\mu\text{-}SbPh_2)(\mu\text{-}H)(\mu_3,\eta^6\text{-}C_6H_4)(Ph)(CO)_{14}$ and $Os_6(\mu_4\text{-}Sb)(\mu\text{-}SbPh_2)(\mu\text{-}H)(\mu_3,\eta^2\text{-}C_6H_4)_2(Ph)(CO)_{16}$ [14]. These clusters are generally products of thermolysis reactions, while **6** was obtained at ambient temperature. A possible driving force for the dephenylation is the conversion of the seven-membered M–P–C–C–C–P–M ring in **4c** to a less strained six-membered ring in **6** [15].

The room temperature $^{31}P\{^1H\}$ and ^1H NMR spectra of **6** suggested the presence of two isomers in solution, in a ratio of about 1.0:0.6. The proposed solution state structures and tentative NMR assignments are given in Scheme 4; the P–P and P–H correlations have been confirmed by both $^1H\{^{31}P\}$ selective decoupling and $^{31}P\{^1H\}$–^1H HMBC experiments. There was no observable $^2J_{PP}$ between the phosphido and phosphine nuclei, consistent with the P(6)–Ru(4)–P(5) bond angle of 84.14(8)°; the coupling constants are expected to follow a Karplus-type relationship [16]. Similar observations have been made with other osmium or ruthenium clusters with P–M–P angles close to 90°; for example, the clusters $Os_3(CO)_6[P(OMe)_3]_6$ (93.3°) [17], $Ru_3(CO)_{10}(\kappa^2\text{-}Ph_2PCH{=}CHPPh_2)$ (85.46°) [18], $H_4Ru_4(CO)_{10}$[1,1-(*R*,*R*)-bdpp] (91.84°) and $H_4Ru_4(CO)_{10}$[1,1-(*S*,*S*)-bdpp] (91.87°) [19], all do not show P–P coupling. An EXSY spectrum taken at 298 K (Fig. 13) showed chemical exchange among the hydrides. A variable

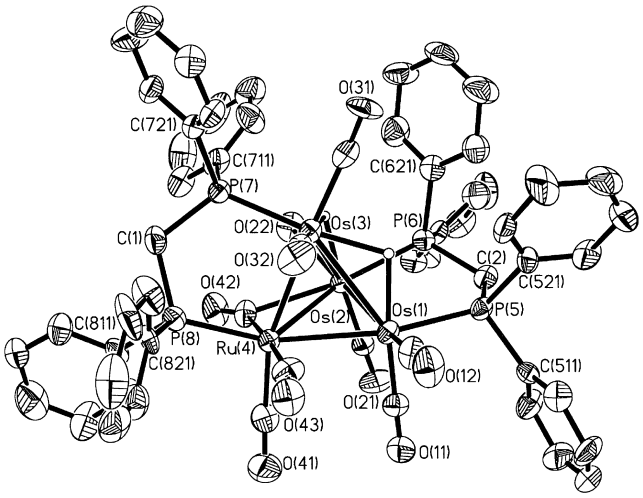

Fig. 10. ORTEP diagram (50% probability thermal ellipsoids, organic hydrogens omitted) and selected bond lengths (Å) and angles (°) for **5**: Os(1)–Os(2) = 2.8027(9); Os(1)–Os(3) = 2.9224(9); Os(1)–Ru(4) = 2.7916(11); Os(2)–Os(3) = 2.9781(9); Os(2)–Ru(4) = 2.8358(11); Os(3)–Ru(4) = 2.8153(11); Os(1)–P(5) = 2.287(4); Os(2)–P(6) = 2.307(4); Os(3)–P(7) = 2.319(4); Ru(4)–P(8) = 2.320(4); P(5)–Os(1)–Os(2) = 95.54(10); P(6)–Os(2)–Os(1) = 89.82(10); P(7)–Os(3)–Ru(4) = 89.78(10); P(8)–Ru(4)–Os(3) = 91.29(10); Ru(4)–C(42)–Os(2) = 79.4(5); O(43)–C(43)–Ru(4) = 169.9(16). Disorder of ruthenium over Os(1), Os(2) and Ru(4).

temperature experiment also showed that all four hydride resonances broadened as the temperature was raised, collapsing into the baseline at 358 K. The proposed exchange pathways are also illustrated in Scheme 4, and involve two separate hydride fluxional processes about an $RuOs_2$ face.

2.4. Minor products

Three minor products were also obtained in this series of reactions, of which only the triosmium cluster $Os_3(\mu\text{-}H)(CO)_9[\mu,\eta^2\text{:}\eta^1\text{-}PPh(CH_2)_2PPh_2]$ (**7**) a minor product from the reaction with dppe, has been characterized crystallographically. The ORTEP plot together with selected bond parameters is given in Fig. 14. The Os(1)–Os(2) distance (2.9437(3) Å) is longer that the other two Os–Os bonds (2.8691(3) and 2.8777(3) Å), and is consistent with those in other related clusters such as $Os_3(\mu\text{-}H)(CO)_{10}(\mu\text{-}PPhR)$ (R = H, Me, Ph), $Os_3(\mu\text{-}H)(CO)_{10}(\mu\text{-}P(C_6F_5)H)$, $Os_3(\mu\text{-}H)(CO)_9\{P(OMe)_3\}(\mu\text{-}PPh_2)$, and $Ru_3(\mu\text{-}H)(CO)_{10}(\mu\text{-}PPhH)$ [20]. The phosphido group bridges the Os(1)–Os(2) edge asymmetrically, with the Os(1)–P(1)–Os(2) plane making a dihedral angle of 109.1° with the metal triangle. One of the axial carbonyl groups bonded to Os(3) deviates from linearity (O(31)–C(31)–Os(3) = 168.6(6)°), most likely the result of steric repulsion by the phenyl ring attached to P(1). The spectroscopic data are consistent with the solid-state structure being retained in solution, and the tentative NMR assignments are given in Fig. 15.

We have ruled out the possibility of $Os_3(\mu\text{-}H)_2(CO)_{10}$, which is known to be a decomposition product from **1**, as the precursor to **7**; its reaction with dppe afforded a pale yellow solid which was found to be insoluble in both hexane and dichloromethane. Thus fragmentation of a dppe-ligated $RuOs_3$ cluster appears to be a more likely pathway.

The reaction with dppm also yielded $RuOs_3(\mu\text{-}H)_2(CO)_{10}(\mu\text{-}CO)_2[\kappa^1\text{-}Ph_2PCH_2P(O)Ph_2]$ (**8**). The infrared spectrum of this complex exhibited a similar carbonyl absorption profile to those of **2**, indicating that the ditertiary phosphine ligand may be bound to the cluster in a κ^1-fashion. The $^{31}P\{^1H\}$ NMR spectrum showed a resonance at δ 23.13 ppm, consistent with those of metal complexes incorporating an oxidized pendant dppm ligand [21]. Although dark red crystals of **8** were obtained and single-crystal X-ray data collected, the data quality was very poor. Nevertheless, the structure solved was in accord with the formulation. The tentative NMR assignments together with the proposed solution state structure for **8** are given in Fig. 15; the correlations have been checked with selective decoupling experiments as well as a $^{31}P\{^1H\}$–^1H HMBC experiment. Although a possible oxidizing agent leading to **8** could have been trimethylamine-*N*-oxide, such cases have been rarely reported [22]; $[Cp_2Rh_2(CO)(\mu,\eta^1\text{:}\eta^1\text{-}CF_3C_2CF_3)\{\kappa^1\text{-}Ph_2P(CH_2)_4PPh_2\}]$ and $[Cr(CO)_5(\kappa^1\text{-dppe})]$ are amongst the few known examples [23,24]. In the latter case it has been suggested that the oxygen transfer may be metal-assisted. A more recent study suggests that oxidation of the pendant phosphine moiety occurs via an intramolecular pathway involving interaction of the uncoordinated phosphorus atom with a carbonyl ligand to form a cyclic intermediate [25].

The cluster **9** is proposed to have the formulation $RuOs_3(\mu\text{-}H)_2(CO)_{10}[\mu_3\text{-}Ph_2PC_{20}H_{12}PPh(C_6H_4)]$. It was obtained in low yields from the reaction with (*S*)-BINAP. Unfortunately, as has been found for **4f**, attempts to grow diffraction-quality crystals of **9** have been unsuccessful. The mass spectrum shows the highest mass ion at *m*/*z* 1576, corresponding to the formula $RuOs_3C_{54}O_{10}H_{33}P_2$. Thermolysis of **4f** afforded **9** in 33% yield, suggesting that **4f** is the precursor to **9**, via orthometallation and expulsion of a carbonyl ligand. Orthometallation of a phenyl group has been observed previously in BINAP-ligated clusters such as $Os_3(\mu\text{-}H)(CO)_8[\mu\text{-}(R)\text{-BINAP-H}]$ [5] and $Ru_3(\mu\text{-}H)(CO)_9\text{-}[\mu_3\text{-}\ Ph_2PC_{20}H_{12}PPh(C_6H_4)]$ [26]. The NMR spectra of **9** pointed to the presence of a single structural species in solution. The tentative assignment of the NMR resonances (Fig. 15) has been obtained with $^1H\{^{31}P\}$ selective decoupling as well as a $^{31}P\{^1H\}$–^1H HMBC spectrum.

2.5. Concluding remarks

In this study, we have shown that the reaction of **1** with ditertiary phosphines gave products in which the ditertiary phosphine ligand either links two metal tetrahedra or bridge a metal–metal bond in a tetrahedral metal framework. Compared with dppm, dppf and BINAP, there appears to be a tendency for dppe, dppp and dppb to link two tetrahedral clusters. This is in line with previous observations that ditertiary phosphines with longer organic

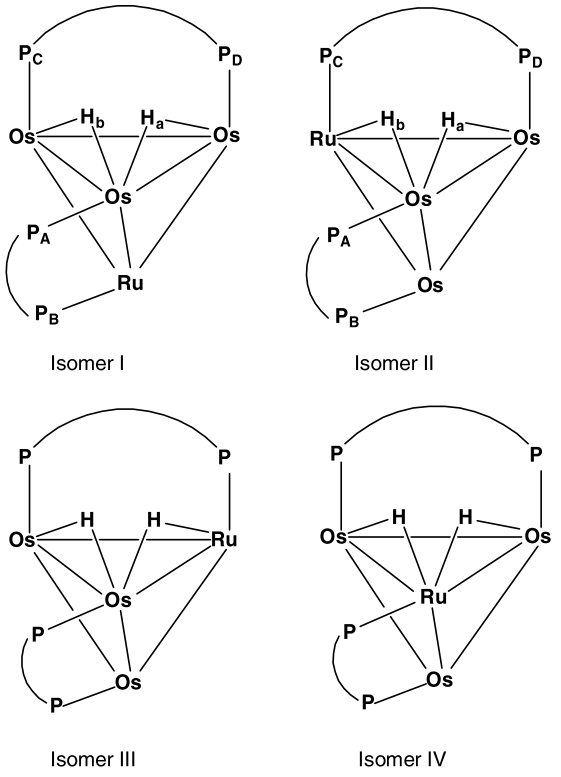

Isomer	P_A (δ)	P_B (δ)	P_C (δ)	P_D (δ)	H_a (δ)	H_b (δ)
I	25.57	-42.04	-40.73	-28.46	-16.87	-19.19
II	-0.69	-4.40	-18.16	-33.77	-16.02	-18.67

Fig. 11. Proposed solution state structures (carbonyls omitted) and tentative (^{31}P and hydride) NMR assignments for **5**.

backbones prefer to form an intermolecular link across two clusters, as opposed to chelating a metal center or bridging a metal–metal bond. The reaction with dppp also afforded **6**, which contains a σ-bonded phenyl group trapped on the cluster. Clusters **4**, **5** and **6**, which incorporated edge-bridging ditertiary phosphine ligands, were found to exist as isomers in solution; there is often a close correlation between the disorder found in the solid-state structures and the isomer distribution in solution. For **4e** and **4f**, there also appear to be conformers resulting from different conformation of the dppf and BINAP backbones.

3. Experimental

3.1. General procedures

All reactions and manipulations were carried out under nitrogen by using standard Schlenk techniques. Solvents were purified, dried, distilled, and stored under nitrogen prior to use. The products were separated by column chromatography on silica gel 60 (230–430 mesh ASTM) and extracted with hexane and dichloromethane. Routine NMR spectra were acquired on a Bruker ACF300 NMR spectrometer, while decoupling and 2D NMR spectra were obtained on a Bruker Avance DRX500 or Bruker AMX500 machine. The solvent used was deuterated chloroform unless otherwise stated. Chemical shifts reported are referenced to that for the residual proton of the solvent for ^{1}H, and to 85% aqueous H_3PO_4 (external standard) for $^{31}P\{^1H\}$. Mass spectra were obtained on a Finnigan MAT95XL-T spectrometer in an *m*-nitrobenzyl alcohol matrix. Microanalyses were carried out by the microanalytical laboratory at the National University of Singapore. The preparation of cluster **1** appears in our earlier report [2a]. All other reagents were from commercial sources and used as supplied.

3.2. Reactions of *1* with ditertiary phosphines

In a typical reaction, a solution of **1** and the ditertiary phosphine in dichloromethane (90 mL) was placed in a three-necked round-bottomed flask and deoxygenated by passing through argon. A solution of $TMNO \cdot 2H_2O$ dissolved in acetonitrile (50 mL) was similarly deoxygenated and then introduced dropwise into the above solution via a pressure-equalizing dropping funnel over 0.5 h. The solu-

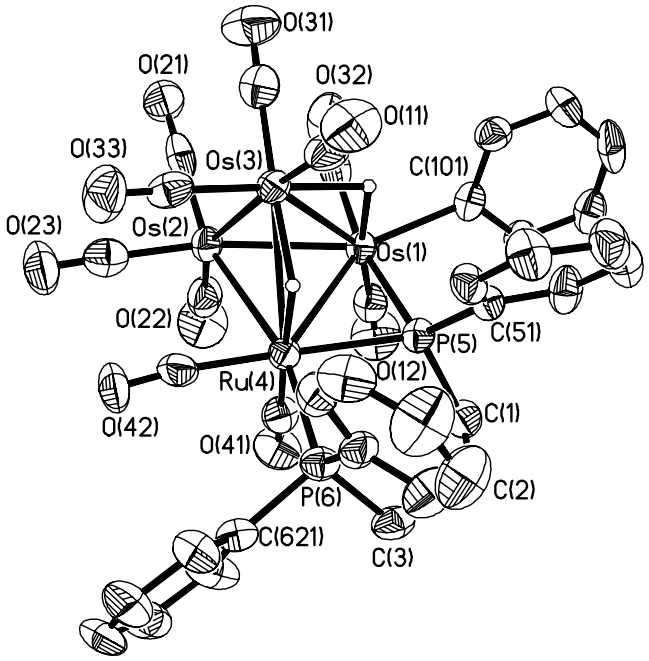

Fig. 12. ORTEP diagram (50% probability thermal ellipsoids, organic hydrogens omitted) and selected bond lengths (Å) and angles (°) for **6**: Os(1)–Os(2) = 2.7781(5); Os(1)–Os(3) = 2.9812(4); Os(1)–Ru(4) = 2.8351(7); Os(2)–Os(3) = 2.7823(5); Os(2)–Ru(4) = 2.8679(7); Os(3)–Ru(4) = 2.9581(7); Os(1)–P(5) = 2.319(2); Ru(4)–P(5) = 2.364(2); Ru(4)–P(6) = 2.360(2); Os(1)–C(101) = 2.160(8); P(5)–Os(1)–Ru(4) = 53.48(5); P(6)–Ru(4)–P(5) = 84.14(8); P(6)–Ru(4)–Os(1) = 135.97(6); P(5)–Ru(4)–Os(1) = 52.01(5).

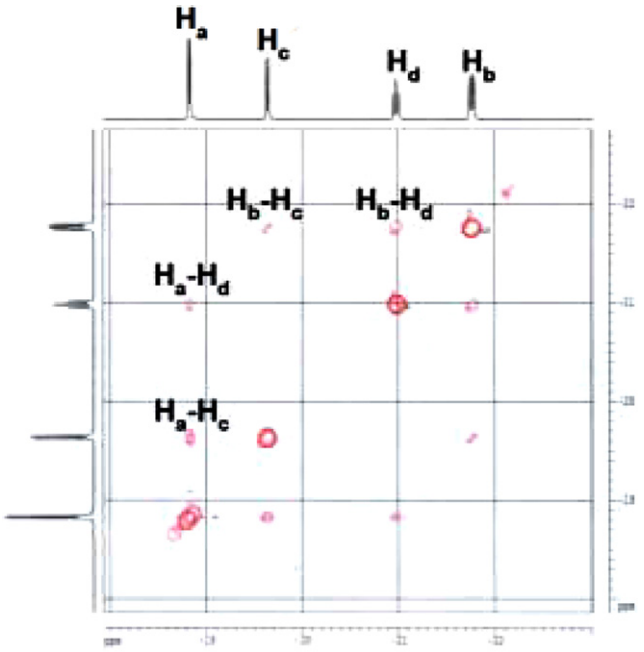

Fig. 13. ^{1}H EXSY for **6** (298 K, $\tau_m = 0.05$ s).

tion was stirred for a further 4.5 h at ambient temperature, and then filtered through a short silica column. Removal of the solvent under reduced pressure was followed by chromatographic separation on silica gel. The reaction conditions and yields are summarized in Table 3.

Compound **2b**: IR (CH_2Cl_2) ν(CO): 2075m, 2033s, 2014m, 2001w, 1989w, 1967w(br) cm^{-1}. ^{31}P{^{1}H} NMR: δ 47.35 (s), 17.33 (s). ^{1}H NMR: δ 7.37–7.16 (m, 20H, Ph), 4.11 (m, 2H, CH_2), 3.96 (m, 2H, CH_2), −21.38 (s, 1H, Ru*H*Os), −21.38 (d, 1H, Ru*H*Os, $^{2}J_{PH} = 8.3$ Hz), −22.06 (s, 1H, Os*H*Os), −22.06 (d, 1H, Os*H*Os, $^{2}J_{PH} = 9.9$ Hz). MS (FAB): *m*/*z* 2421 (M^+), calcd for M^+: 2418. Anal. Calc. for $C_{50}H_{28}O_{24}Os_6P_2Ru \cdot 0.5C_6H_{14}$: C, 25.86; H, 1.43. Found: C, 25.81; H, 1.36%. Presence of hexane in the analytical sample was verified by ^{1}H NMR spectroscopy.

Compound **2c**: IR (CH_2Cl_2) ν(CO): 2092m, 2064vs, 2037vs, 2020s, 1999m(sh) cm^{-1}. ^{31}P{^{1}H} NMR: δ 39.91 (s). ^{1}H NMR: δ 7.48–7.30 (m, 20H, Ph), 2.75 (m, 2H, CH_2), 2.31 (m, 2H, CH_2), 2.04 (m, 2H, CH_2), −20.25 (s, 2H, Os*H*Os), −21.48 (d, 2H, Ru*H*Os, $^{2}J_{PH} = 11.6$ Hz). MS(FAB): *m*/*z* 2432 (M^+), calcd for M^+: 2432. Anal. Calc. for $C_{51}H_{30}O_{24}Os_6P_2Ru_2 \cdot C_6H_{14}$: C, 27.18; H, 1.76. Found: C, 27.58; H, 1.99%. Presence of hexane in the analytical sample was verified by ^{1}H NMR spectroscopy.

Compound **2d**: IR (CH_2Cl_2) ν(CO): 2093m, 2063vs, 2037vs, 2021s, 2007m, 1994m(sh) cm^{-1}. ^{31}P{^{1}H} NMR: δ 39.37 (s). ^{1}H NMR: δ 7.45 (s, 20H, Ph), 2.59 (s, 4H, CH_2), 2.35 (s, 2H, CH_2), 2.04 (s, 2H, CH_2), −19.91 (s,

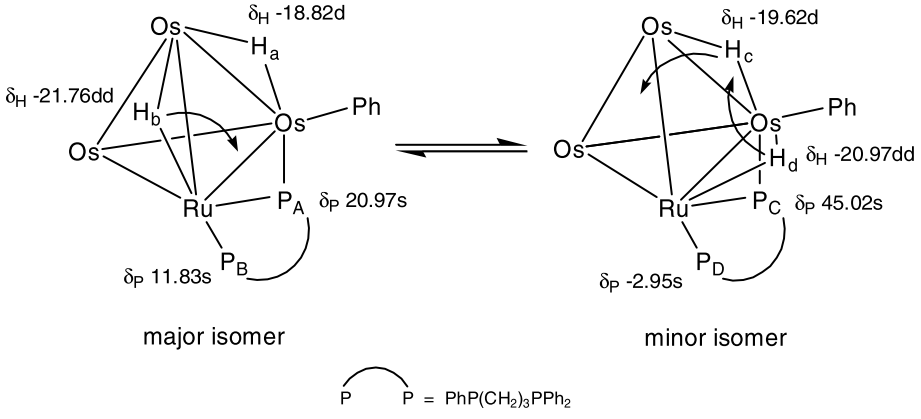

Scheme 4.

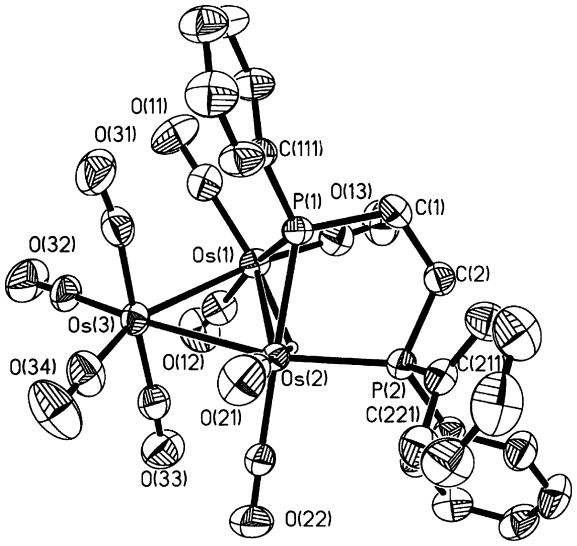

Fig. 14. ORTEP diagram (50% probability thermal ellipsoids, organic hydrogens omitted) and selected bond lengths (Å) and angles (°) for **7**: Os(1)–Os(3) = 2.8691(3); Os(1)–Os(2) = 2.9437(3); Os(2)–Os(3) = 2.8777(3); Os(1)–P(1) = 2.3779(14); Os(2)–P(1) = 2.3483(14); Os(2)–P(2) = 2.3233(14); P(1)–Os(1)–Os(2) = 51.03(3); P(2)–Os(2)–P(1) = 83.39(5); P(2)–Os(2)–Os(1) = 104.55(4); P(1)–Os(2)–Os(1) = 51.93(4); Os(2)–P(1)–Os(1) = 77.05(4); O(31)–C(31)–Os(3) = 168.6(6).

2H, Os*H*Os), −21.54 (d, 2H, Ru*H*Os, $^2J_{PH} = 9.9$ Hz). MS (FAB): *m*/*z* 2446 (M^+), calcd for M^+: 2446. Anal. Calc. for $C_{50}H_{32}O_{22}Os_6P_2Ru_2 \cdot C_6H_{14}$: C, 27.16; H, 1.87. Found: C, 27.12; H, 1.69%. Presence of hexane in the analytical sample was verified by ^{1}H NMR spectroscopy..

Compound **3**: IR (CH_2Cl_2) *ν*(CO): 2072s, 2042vs, 2007vs, 2000vs, 1985m, 1964w, 1770vw(br) cm^{-1}. $^{31}P\{^1H\}$ NMR: *δ* 41.82 (s), 10.05 (s). ^{1}H NMR: *δ* 7.44–7.29 (m, 40H, Ph), 4.18 (m, 2H, CH_2), 3.99 (m, 2H, CH_2), 2.13 (m, 2H, CH_2), 2.05 (m, 2H, CH_2), 1.81 (m, 1H, CH_2), 1.72 (m, 1H, CH_2), 0.80 (m, 1H, CH_2), 0.75 (m, 1H, CH_2), −21.29 (d, 2H, Ru*H*Os, $^2J_{PH} = 11.6$ Hz), −21.96 (d, 2H, Os*H*Os, $^2J_{PH} = 11.6$ Hz). MS (FAB): *m*/*z* 2789 (M^+), calcd for M^+: 2788. Anal. Calc. for $C_{76}H_{56}O_{22}Os_6P_4Ru_2$: C, 32.73; H, 2.02. Found: C, 32.69; H, 2.05%.

Compound **4a**: IR (CH_2Cl_2) *ν*(CO): 2078m, 2043s, 2007vs, 1979mw, 1943w, 1811vw(br) cm^{-1}. $^{31}P\{^1H\}$ NMR: *δ* −35.92 (s) [major isomer]; −12.41 (d, $^2J_{PP} = 24.8$ Hz), −34.50 (d) [minor isomer]. ^{1}H NMR: *δ* 7.42–7.30 (m, 20H, Ph), 6.67 (m, 1H, CH_2), 5.04 (m, 1H, CH_2), −19.60 (d, 2H, Os*H*Os, $^2J_{PH} = 8.2$ Hz) [major isomer]; 7.24–7.21 (m, 20H, Ph), 6.45 (m, 1H, CH_2), 5.00 (m, 1H, CH_2), −18.70 (d, 1H, Ru*H*Os, $^2J_{PH} = 9.1$ Hz), −19.45 (d, 1H, Os*H*Os, $^2J_{PH} = 9.1$ Hz) [minor isomer].

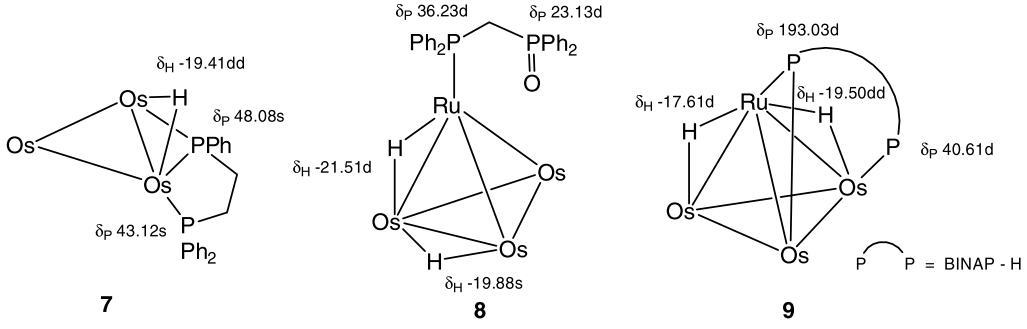

Fig. 15. Proposed solution state structures (carbonyls omitted) and tentative (^{31}P and hydride) NMR assignments for **7**, **8** and **9**.

Table 3
Reactions of **1** with ditertiary phosphines

Amount of **1**	Ligand	Amount of ligand	Amount of TMNO · $2H_2O$	Product	Color	Yield
49.1 mg, 0.047 mmol	dppm	18.2 mg, 0.047 mmol	10.9 mg, 0.098 mmol	**8**	Dark red	4.1 mg, 6%
				4a	Dark red	36.6 mg, 57%
				5	Dark brown	12.2 mg, 15%
44.5 mg, 0.043 mmol	dppe	17.0 mg, 0.043 mmol	9.3 mg, 0.084 mmol	**7**	Yellow	5.4 mg, 11%
				2b	Dark orange	27.2 mg, 52%
56.7 mg, 0.055 mmol	dppp	23.1 mg, 0.056 mmol	12.1 mg, 0.110 mmol	**2c**	Dark orange	22.1 mg, 33%
				6	Purplish-red	32.4 mg, 40%
				3	Purplish-red	13.8 mg, 18%
60.2 mg, 0.058 mmol	dppb	24.7 mg, 0.059 mmol	13.0 mg, 0.117 mmol	**2d**	Dark orange	31.2 mg, 44 %
				4d	Dark orange	32.7 mg, 40%
60.1 mg, 0.058 mmol	dppf	32.1 mg, 0.058 mmol	13.0 mg, 0.117 mmol	**4e**	Dark orange	70.7 mg, 79%
40.2 mg, 0.039 mmol	(*S*)-BINAP	24.1 mg, 0.039 mmol	8.8 mg, 0.079 mmol	**9**	Dark orange	10.1 mg, 16%
				4f	Dark orange	42.8 mg, 69%

MS (FAB): *m/z* 1368 (M^+), calcd for M^+: 1366. Anal. Calc. for $C_{36}H_{24}O_{11}Os_3P_2Ru \cdot CH_2Cl_2$: C, 30.60; H, 1.79. Found: C, 30.45; H, 1.96%. Presence of dichloromethane in the analytical sample was verified by ^1H NMR spectroscopy.

Compound **4d**: IR (CH_2Cl_2) *ν*(CO): 2075m, 2032s, 2017m, 1999mw, 1989w(sh), 1965w cm^{-1}. $^{31}P\{^1H\}$ NMR: *δ* 18.10 (s), 3.31 (s) [major isomer]; 34.08 (s), −3.09 (s) [minor isomer]. ^1H NMR: *δ* 7.60–7.32 (m, 20H, Ph), 3.36 (m, 2H, CH_2), 2.66 (m, 2H, CH_2), 2.46 (m, 2H, CH_2), 2.25 (m, 2H, CH_2), −18.36 (d, 1H, Ru*H*Os, $^2J_{PH} = 9.2$ Hz), −21.46 (dd, 1H, Ru*H*Os, $^2J_{PH} = 13.8$ Hz, $^2J_{PH} = 7.7$ Hz) [major isomer]; 7.60–7.32 (m, 20H, Ph), 3.27 (m, 2H, CH_2), 2.63 (m, 2H, CH_2), 2.44 (m, 2H, CH_2), 2.27 (m, 2H, CH_2), −19.24 (d, 1H, Os*H*Os, $^2J_{PH} = 13.7$ Hz), −20.80 (dd, 1H, Ru*H*Os, $^2J_{PH} = 13.8$ Hz, $^2J_{PH} = 9.2$ Hz) [minor isomer]. MS (FAB): *m/z* 1408 (M^+), calcd for M^+: 1408. Anal. Calc. for $C_{39}H_{30}O_{11}Os_3P_2Ru \cdot 0.5C_6H_{14}$: C, 34.78; H, 2.50. Found: C, 34.60; H, 2.41%. Presence of hexane in the analytical sample was verified by ^1H NMR spectroscopy.

Compound **4e**: IR (CH_2Cl_2) *ν*(CO): 2075s, 2034vs, 2016s, 2002m, 1988m, 1967m cm^{-1}. $^{31}P\{^1H\}$ NMR (223 K): *δ* 22.23 (s), 4.40 (s) [isomer I]; 18.59 (s), 8.45 (s) [isomer II]; 40.06 (s), −2.70 (s) [isomer III]; 44.74 (s), −7.97 (s) [isomer IV]. ^1H NMR (223 K): *δ* 7.80–7.74 (m, 5H, Ph), 7.56–7.55 (m, 5H, Ph), 7.22–7.16 (m, 5H, Ph), 7.03–7.05 (m, 5H, Ph), 4.41 (s, 4H, C_5H_4), 4.01 (s, 2H, C_5H_4), 3.56 (s, 2H, C_5H_4), −18.16 (d, 1H, Ru*H*Os, $^2J_{PH} = 2.1$ Hz), −20.42 (dd, 1H, Ru*H*Os, $^2J_{PH} = 14.7$ Hz, $^2J_{PH} = 7.4$ Hz) [isomer I]; 7.68–7.64 (m, 5H, Ph), 7.33–7.22 (m, 10H, Ph), 7.22–7.16 (m, 5H, Ph), 4.80 (s, 2H, C_5H_4), 4.34 (s, 2H, C_5H_4), 4.28 (s, 2H, C_5H_4), 4.07 (s, 2H, C_5H_4), −17.55 (d, 1H, Ru*H*Os, $^2J_{PH} = 10.5$ Hz) −20.24 (dd, 1H, Ru*H*Os, $^2J_{PH} = 8.2$ Hz, $^2J_{PH} = 5.7$ Hz) [isomer II]; 7.80–7.74 (m, 5H, Ph), 7.51–7.44 (m, 5H, Ph), 7.22–7.17 (m, 5H, Ph), 7.16–7.94 (m, 5H, Ph), 4.52 (s, 2H, C_5H_4), 4.37 (s, 2H, C_5H_4), 3.75 (d, 2H, C_5H_4), 3.63 (s, 2H, C_5H_4), −18.89 (d, 1H, Os*H*Os, $^2J_{PH} = 7.4$ Hz), −19.33 (dd, 1H, Ru*H*Os, $^2J_{PH} = 14.7$ Hz, $^2J_{PH} = 10.5$ Hz) [isomer III]; 7.68–7.64 (m, 10H, Ph), 7.22–7.17 (m, 10H, Ph), 4.37 (s, 4H, C_5H_4), 4.19 (s, 2H, C_5H_4), 4.16 (s, 2H, C_5H_4), −18.29 (d, 1H, Os*H*Os, $^2J_{PH} = 12.6$ Hz), −19.54 (dd, 1H, Ru*H*Os, $^2J_{PH} = 10.5$ Hz, $^2J_{PH} = 9.0$ Hz) [isomer IV]. MS (FAB): *m/z* 1537 (M^+), calcd for M^+: 1536. Anal. Calc. for $C_{45}H_{30}FeO_{11}Os_3P_2Ru \cdot 0.25CH_2Cl_2$: C, 34.90; H, 1.97. Found: C, 34.95; H, 2.03%. Presence of dichloromethane in the analytical sample was verified by ^1H NMR spectroscopy.

Compound **4f**: IR (CH_2Cl_2) *ν*(CO): 2075s, 2033s, 2017s, 2001m, 1988m, 1967m cm^{-1}. $^{31}P\{^1H\}$ NMR (183 K): *δ* 47.24 (s), 8.98 (s) [isomer I]; 30.27 (s), 15.81 (s) [isomer II]; 46.30 (s), 22.83 (s) [isomer III]; 51.13 (s), 7.04 (s) [isomer IV]; 31.47 (s), 19.71 (s) [isomer V]; 192.61(s), 45.34 (s) [isomer VI]; 55.17 (s), 6.46 (s) [isomer VII]. ^1H NMR (183 K): *δ* 8.11–5.83 (m, 32H, Ph and naphthyl), −18.05 (d, 1H, Ru*H*Os, $^2J_{PH} = 7.9$ Hz), −19.63 (dd, 1H, Ru*H*Os, $^2J_{PH} = 17.3$ Hz, $^2J_{PH} = 17.3$ Hz) [isomer I]; 8.11–5.83 (m, 32H, Ph and naphthyl), −17.46 (d, 1H, Ru*H*Os, $^2J_{PH} = 5.0$ Hz), −19.74 (dd, 1H, Ru*H*Os, $^2J_{PH} = 15.8$ Hz, $^2J_{PH} = 23.6$ Hz) [isomer II]; 8.11–5.83 (m, 32H, Ph and naphthyl), −18.48 (d, 1H, Os*H*Os, $^2J_{PH} = 10.9$ Hz), −19.19 (dd, 1H, Ru*H*Os, $^2J_{PH} = 15.3$ Hz, $^2J_{PH} = 20.2$ Hz) [isomer III]; 8.11–5.83 (m, 32H, Ph and naphthyl), −18.15 (d, 1H, Os*H*Os, $^2J_{PH} = 6.9$ Hz), −18.58 (dd, 1H, Ru*H*Os, $^2J_{PH} = 17.8$ Hz, $^2J_{PH} = 23.6$ Hz) [isomer IV]; 8.11–5.83 (m, 32H, Ph and naphthyl), −18.21 (d, 1H, Ru*H*Os, $^2J_{PH} = 6.9$ Hz), −18.35 (dd, 1H, Ru*H*Os, $^2J_{PH} = 9.9$ Hz, $^2J_{PH} = 25.6$ Hz) [isomer V]; 8.11-5.83 (m, 32H, Ph and naphthyl), −19.03 (d, 1H, Os*H*Os, $^2J_{PH} = 9.9$ Hz), −19.55 (dd, 1H, Ru*H*Os, $^2J_{PH} = 7.8$ Hz, $^2J_{PH} = 5.0$ Hz) [isomer VI]; 8.11-5.83 (m, 32H, Ph and naphthyl), −18.56 (d, 1H, Os*H*Os, $^2J_{PH} = 4.9$ Hz), (dd not resolved) [isomer VII]. MS (FAB): *m/z* 1605 (M^+), calcd for M^+: 1605. Anal. Calc. for $C_{55}H_{34}O_{11}Os_3P_2Ru \cdot 1.5C_6H_{14}$: C, 44.33; H, 3.20. Found: C, 44.08; H, 3.03%. Presence of hexane in the analytical sample was verified by ^1H NMR spectroscopy.

Compound **5**: IR (CH_2Cl_2) *ν*(CO): 2021m, 1993vs, 1982s, 1953m, 1932w cm^{-1}. $^{31}P\{^1H\}$ NMR: 25.57 (dd, $^2J_{PP} = 53.4$ Hz, $^3J_{PP} = 11.5$ Hz), −28.46 (d, $^2J_{PP} = 26.7$ Hz), −40.73 (dd, $^2J_{PP} = 26.7$ Hz, $^3J_{PP} = 11.5$ Hz), −42.04 (d, $^2J_{PP} = 53.4$ Hz) [major isomer]; −0.69 (dd, $^2J_{PP} = 45.8$ Hz, $^3J_{PP} = 7.6$ Hz), −4.40 (d, $^2J_{PP} = 45.8$ Hz), −18.16 (dd, $^2J_{PP} = 26.7$ Hz, $^3J_{PP} = 7.6$ Hz), −33.77 (d, $^2J_{PP} = 26.7$ Hz) [minor isomer]. ^1H NMR: 7.67–6.42 (m, 40H, Ph), 4.93 (m, 4H, CH_2), −16.87 (dd, 1H, Os*H*Os, $^2J_{PH} = 30.9$ Hz, $^2J_{PH} = 10.7$ Hz), −19.19 (dd, 1H, Os*H*Os, $^2J_{PH} = 9.9$ Hz, $^2J_{PH} = 9.9$ Hz) [major isomer]; 7.67–6.42 (m, 40H, Ph), 4.93 (m, 4H, CH_2), −16.02 (dd, 1H, Os*H*Os, $^2J_{PH} = 31.3$ Hz, $^2J_{PH} = 10.7$ Hz), −18.67 (dd, 1H, Ru*H*Os, $^2J_{PH} = 9.9$ Hz, $^2J_{PH} = 9.9$ Hz) [minor isomer]. MS (FAB): *m/z* 1695 (M^+), calcd for M^+: 1695. Anal. Calc. for $C_{59}H_{46}O_9Os_3P_4Ru \cdot 0.5C_6H_{14} \cdot 0.75CH_2Cl_2$: C, 41.80; H, 3.03. Found: C, 41.70; H, 2.73%. Presence of hexane and dichloromethane in the analytical sample was verified by ^1H NMR spectroscopy.

Compound **6**: IR (CH_2Cl_2) *ν*(CO): 2075vs, 2041vs, 2034s, 2018vs, 2009 s(sh), 1989m, 1965w cm^{-1}. $^{31}P\{^1H\}$ NMR: *δ* 20.97 (s, PPh), 11.84 (s, PPh_2) [major isomer]; 45.02 (s, PPh), −2.95 (s, PPh_2) [minor isomer]. ^1H NMR: *δ* 7.60–7.52 (m, 15H, Ph), 7.26 (s, 5H, Ph), 3.48 (m, 2H, CH_2), 2.49 (m, 2H, CH_2), 2.40 (m, 2H, CH_2), −18.82 (d, 1H, Os*H*Os, $^2J_{PH} = 9.1$ Hz), −21.76 (dd, 1H, Ru*H*Os, $^2J_{PH} = 14.7$ Hz, $^2J_{PH} = 10.2$ Hz) [major isomer]; 7.60–7.52 (m, 15 H, Ph), 7.26 (s, 5H, Ph), 3.22 (m, 2H, CH_2), 2.68 (m, 2H, CH_2), 2.36 (m, 2H, CH_2), −19.62 (d, 1H, Os*H*Os, $^2J_{PH} = 11.3$ Hz), −20.97 (dd, 1H, Ru*H*Os, $^2J_{PH} = 14.7$ Hz, $^2J_{PH} = 12.4$ Hz) [minor isomer]. MS (FAB): *m/z* 1395 $(M \cdot CH_2Cl_2 - 2CO)^+$, calcd for M^+: 1451. Anal. Calc. for $C_{37}H_{28}O_{10}Os_3P_2Ru$: C, 32.53; H, 2.07. Found: C, 32.74; H, 1.87%.

Compound **7**: IR (CH_2Cl_2) *ν*(CO): 2090m, 2044s, 2012vs, 1999m, 1977w, 1966m cm^{-1}. $^{31}P\{^1H\}$ NMR: *δ* 48.08 (s), 43.12 (s). ^1H NMR: *δ* 7.62–7.36 (m, 15H, Ph), 2.46 (m,

2H, CH_2), 2.32 (m, 2H, CH_2), −19.41 (dd, 1H, Os*H*Os, $^2J_{PH} = 16.5$ Hz, $^2J_{PH} = 8.3$ Hz). MS (ESI): *m*/*z* 1145 (M^-), calcd for M^-: 1145. Anal. Calc. for $C_{29}H_{20}O_9Os_3P_2$: C, 30.42; H, 1.76. Found: C, 30.16; H, 1.85%.

Compound **8**: IR (CH_2Cl_2) *ν*(CO): 2093m, 2064vs, 2037s, 2031ms, 2006m(br), 1970 w(br) cm^{-1}. $^{31}P\{^1H\}$ NMR: *δ* 36.23 (d, $^2J_{PP} = 11.5$ Hz), 23.13 (d). ^1H NMR: *δ* 7.70–7.38 (m, 20H, Ph), 4.21 (m, 1H, CH_2), 3.82 (m, 1H, CH_2), −19.88 (s, 1H, Ru*H*Os), −21.51 (d, 1H, Os*H*Os, $^2J_{PH} = 9.9$ Hz). MS (FAB): *m*/*z* 1410 (M^+), calcd for M^+: 1410. Anal. Calc. for $C_{37}H_{24}O_{13}Os_3P_2Ru$: C, 31.49; H, 1.70. Found: C, 31.74; H, 1.89%.

Compound **9**: IR (CH_2Cl_2) *ν*(CO): 2077s, 2044s, 2018m, 1990w(br) cm^{-1}. $^{31}P\{^1H\}$ NMR: *δ* 193.03 (s), 40.61 (s). ^1H NMR: *δ* 7.81–7.09 (m, 32H, Ph and naphthyl), −17.61 (d, 1H, Ru*H*Os, $^2J_{PH} = 7.6$ Hz), −19.50 (dd, 1H, Ru*H*Os, $^2J_{PH} = 7.7$ Hz, $^2J_{PH} = 7.7$ Hz). MS (FAB): *m*/*z* 1576 (M^+), calcd for M^+: 1576. Anal. Calc. for $C_{54}H_{33}O_{10}Os_3P_2Ru \cdot C_6H_{14}$: C, 43.32; H, 2.83. Found: C, 43.77; H, 3.33%. Presence of hexane in the analytical sample was verified by ^1H NMR spectroscopy.

3.3. Reaction of *2c* with dppp

A solution of **2c** (11.4 mg, 0.005 mmol) and dppp (2.5 mg, 0.006 mmol) in dichloromethane (50 mL) was placed in a three-necked round-bottomed flask and deoxygenated by passing through argon. A solution of $TMNO.2H_2O$ (1.3 mg, 0.012 mmol) dissolved in acetonitrile (25 mL) was similarly deoxygenated and then introduced dropwise into the above solution via a pressure-equalizing dropping funnel over 0.5 h. The solution was stirred for a further 4.5 h at ambient temperature. Unreacted **2c** was recovered quantitatively after work-up as above.

3.4. Thermolysis of *4f*

To a Schlenk tube containing **4f** (11.1 mg, 0.007 mmol) was added cyclohexane (30 mL), and the reaction mixture was stirred and refluxed for 6 h. Subsequent work-up as above afforded unreacted **4f** (6.2 mg) and **9** (3.6 mg, 33%), respectively.

3.5. X-ray crystal structure determinations

Crystals were mounted on quartz fibres. X-ray data were collected on a Bruker AXS APEX system, using Mo Kα radiation, at 223 K with the SMART suite of programs [27]. Data were processed and corrected for Lorentz and polarization effects with SAINT [28], and for absorption effects with SADABS [29]. Structural solution

Table 4
Crystal data for **2b**–**d** and **3**

Compound	**2b**	**2c**	**2d**	**3**
Formula	$C_{50}H_{28}O_{24}Os_6P_2Ru_2 \cdot CH_2Cl_2$	$C_{51}H_{30}O_{24}Os_6P_2Ru_2$	$C_{52}H_{32}O_{24}Os_6P_2Ru_2$	$C_{76}H_{56}O_{22}Os_6P_4Ru_2 \cdot CH_2Cl_2$
F_W	2502.92	2432.03	2446.06	2873.35
Crystal system	Triclinic	Triclinic	Triclinic	Monoclinic
Space group	$P\bar{1}$	$P\bar{1}$	$P\bar{1}$	$P2_1/c$
Unit cell dimensions				
a (Å)	9.7376(4)	13.5739(17)	8.8999(4)	20.6320(5)
b (Å)	10.5139(4)	15.1359(19)	12.4626(6)	13.8492(4)
c (Å)	16.9081(7)	16.237(2)	15.2787(7)	31.7821(8)
α (°)	73.4400(10)	76.547(3)	93.631(1)	90
β (°)	83.1130(10)	81.878(3)	103.083(1)	107.6630(10)
γ (°)	84.4810(10)	85.908(2)	110.548(1)	90
Volume ($Å^3$)	1643.78(11)	3209.4(7)	1526.59(12)	8653.2(4)
Z	2	2	1	4
ρ_c (mg m^{-3})	2.528	2.517	2.661	2.206
μ(Mo Kα) (mm^{-1})	12.194	12.407	13.042	9.315
F(000)	1136	2204	1110	5336
Crystal size (mm)	0.10 × 0.10 × 0.02	0.06 × 0.12 × 0.12	0.28 × 0.12 × 0.08	0.22 × 0.12 × 0.08
θ Range (°)	2.03–28.28	2.01–26.37	2.07–26.37	2.03–29.95
Reflections collected	22 583	37 513	22 747	70 697
Independent reflections [R_{int}]	7991	13 104	6245	23 040
Completeness %, (to *θ*, °)	98.2 (28.28)	99.9 (26.37)	99.9 (26.37)	91.7 (29.95)
Transmission range	0.647–0.383	0.431–0.241	0.422–0.121	0.493–0.318
Data/restraints/parameters	7991/6/396	13 104/0/445	6245/0/388	23 040/0/1045
Goodness-of-fit on F^2	1.025	1.121	1.045	0.826
Final *R* indices [$I > 2\sigma(I)$]	$R_1 = 0.0494$, $wR_2 = 0.1342$	$R_1 = 0.0913$, $wR_2 = 0.2021$	$R_1 = 0.0297$, $wR_2 = 0.0721$	$R_1 = 0.0505$, $wR_2 = 0.0825$
R indices (all data)	$R_1 = 0.0680$, $wR_2 = 0.1419$	$R_1 = 0.1320$, $wR_2 = 0.2214$	$R_1 = 0.0351$, $wR_2 = 0.0747$	$R_1 = 0.1223$, $wR_2 = 0.0956$
Largest difference in peak and hole (e $Å^{-3}$)	3.125 and –1.828	4.862 and –1.538	1.586 and –1.574	2.182 and –1.041

Table 5
Crystal data for **4a**, **4d** and **4e**

Compound	**4a**	**4d**	**4e**
Formula	$C_{36}H_{24}O_{11}Os_3P_2Ru \cdot CH_2Cl_2$	$C_{39}H_{30}O_{11}Os_3P_2Ru$	$C_{45}H_{30}FeO_{11}Os_3P_2Ru \cdot 1/4CH_2Cl_2$
F_W	1451.09	1408.24	1557.38
Crystal system	Monoclinic	Monoclinic	Triclinic
Space group	$P2_1/n$	$C2/c$	$P\bar{1}$
Unit cell dimensions			
a (Å)	18.3499(4)	37.7049(9)	9.9177(5)
b (Å)	12.0405(3)	10.6137(3)	12.0995(6)
c (Å)	18.6689(3)	28.7725(7)	20.7735(10)
α (°)	90	90	81.7990(10)
β (°)	95.5050(10)	125.2140(10)	84.7800(10)
γ (°)	90	90	68.0000(10)
Volume (Å^3)	4105.72(15)	9407.3(4)	2285.7(2)
Z	4	8	2
ρ_c (mg m^{-3})	2.348	1.989	2.263
μ(Mo Kα) (mm^{-1})	9.880	8.511	9.099
F(000)	2688	5232	1453
Crystal size (mm)	$0.30 \times 0.26 \times 0.14$	$0.36 \times 0.30 \times 0.16$	$0.34 \times 0.18 \times 0.12$
θ Range (°)	2.02–30.50	2.03–29.97	2.18–30.00
Reflections collected	37237	43312	34099
Independent reflections (R_{int})	11805	13387	12831
Completeness %, (to θ, °)	94.2 (30.50)	97.9 (29.97)	96.4 (30.00)
Transmission range	0.266–0.132	0.343–0.150	0.408–0.148
Data/restraints/parameters	11805/1/507	13387/0/506	12831/2/577
Goodness-of-fit on F^2	0.831	1.057	1.027
Final R indices [$I > 2\sigma(I)$]	$R_1 = 0.0369$, $wR_2 = 0.0674$	$R_1 = 0.0320$, $wR_2 = 0.0832$	$R_1 = 0.0339$, $wR_2 = 0.0861$
R indices (all data)	$R_1 = 0.0645$, $wR_2 = 0.0712$	$R_1 = 0.0438$, $wR_2 = 0.0878$	$R_1 = 0.0441$, $wR_2 = 0.0900$
Largest difference in peak and hole (e Å^{-3})	1.943 and –1.100	2.217 and –0.679	2.468 and –0.947

Table 6
Crystal data for **5**, **6** and **9**

Compound	**5**	**6**	**7**
Formula	$C_{59}H_{46}O_9Os_3P_4Ru \cdot 3/4CH_2Cl_2 \cdot 1/2C_6H_{14}$	$C_{37}H_{28}O_{10}Os_3P_2Ru \cdot CH_2Cl_2$	$C_{29}H_{20}O_9Os_3P_2 \cdot 1/2CH_2Cl_2$
F_W	1801.29	1451.13	1187.45
Crystal system	Monoclinic	Triclinic	Monoclinic
Space group	$I2/a$	$P\bar{1}$	$C2/c$
Unit cell dimensions			
a (Å)	22.4887(14)	11.0569(5)	30.2200(5)
b (Å)	21.2407(12)	12.1951(6)	12.0104(2)
c (Å)	27.7515(17)	17.1442(8)	18.5905(3)
α (°)	90	79.5610(10)	90
β (°)	102.977(3)	71.3020(10)	100.0640
γ (°)	90	74.8740(10)	90
Volume (Å^3)	12917.7(13)	2101.79(17)	6643.68(19)
Z	8	2	8
ρ_c (mg m^{-3})	1.852	2.293	2.374
μ(Mo Kα) (mm^{-1})	6.326	9.649	11.673
F(000)	6884	1348	4360
Crystal size (mm)	$0.05 \times 0.14 \times 0.32$	$0.12 \times 0.10 \times 0.08$	$0.24 \times 0.22 \times 0.18$
θ Range (°)	2.08–26.37	2.03–30.51	2.08–30.48
Reflections collected	95146	26565	30623
Independent reflections (R_{int})	13213	11962	9622
Completeness %, (to θ, °)	99.9 (26.37)	93.2 (30.51)	95.0 (30.48)
Transmission range	0.647–0.359	0.528–0.419	0.213–0.126
Data/restraints/parameters	13213/10/733	11962/0/505	9622/0/399
Goodness-of-fit on F^2	0.962	0.740	0.860
Final R indices [$I > 2\sigma(I)$]	$R_1 = 0.0620$, $wR_2 = 0.1688$	$R_1 = 0.0466$, $wR_2 = 0.0730$	$R_1 = 0.0349$, $wR_2 = 0.0644$
R indices (all data)	$R_1 = 0.1185$, $wR_2 = 0.1918$	$R_1 = 0.0971$, $wR_2 = 0.0819$	$R_1 = 0.0530$, $wR_2 = 0.0681$
Largest difference in peak and hole (e Å^{-3})	3.024 and –1.047	1.642 and –1.267	1.528 and –1.013

and refinement were carried out with the SHELXTL suite of programs [30]. Crystal and refinement data are summarized in Tables 4–6.

The structures were solved either by direct methods or Patterson maps to locate the heavy atoms, followed by difference maps for the light, non-hydrogen atoms. The hydrides were placed by potential energy calculations with the program XHYDEX [31], given fixed isotropic thermal parameters, and refined riding on one of the heavy atom to which they are attached. Organic hydrogen atoms were placed in calculated positions and refined with a riding model. All non-hydrogen atoms were generally given anisotropic displacement parameters in the final model, except for **2c**. The crystal of **2c** diffracted rather weakly, resulting in a rather poor data set, which may account for the large residues. The carbon atoms in **2c** were assigned isotropic thermal parameters, and restraints placed on the phenyl rings. The molecules of **2b** and **2d** sit on special positions (center of symmetry), and with the exception of clusters **2c**, **6** and **7**, the clusters exhibited disorder of the heavy atom positions. Solvent molecules were also located in **2b**, **4a**, **4e**, **5**, **6** and **7**. Details of the modelling of disorder and treatment of solvent molecules are given in Supplementary material.

Acknowledgements

This work was supported by the National University of Singapore (Research Grant No. R143-000-267-112) and one of us (Y.L.K.T.) thanks the University for a Research Scholarship.

Appendix A. Supplementary material

CCDC 627114, 627115, 627116, 627117, 627118, 627119, 627120, 627121, 627122 and 627123 contain the supplementary crystallographic data for this paper. These data can be obtained free of charge via http://www.ccdc.cam.ac.uk/conts/retrieving.html, or from the Cambridge Crystallographic Data Centre, 12 Union Road, Cambridge CB2 1EZ, UK; fax: (+44) 1223-336-033; or e-mail: deposit@ccdc.cam.ac.uk. Supplementary data associated with this article can be found, in the online version, at doi:10.1016/j.jorganchem.2007.02.001.

References

[1] (a) J.R. Fox, W.L. Gladfelter, T.G. Wood, J.A. Smegal, T.K. Foreman, G.L. Geoffroy, I. Tavaniepour, V.W. Day, C.S. Day, Inorg. Chem. 20 (1981) 3214–3223;
(b) W.L. Gladfelter, J.R. Fox, J.A. Smegal, T.G. Wood, G.L. Geoffroy, Inorg. Chem. 20 (1981) 3223–3229;
(c) W.L. Gladfelter, G.L. Geoffroy, Inorg. Chem. 19 (1980) 2574–2578;
(d) J.R. Fox, W.L. Gladfelter, G.L. Geoffroy, Inorg. Chem. 19 (1980) 2579–2585.

[2] (a) L. Pereira, W.K. Leong, S.Y. Wong, J. Organomet. Chem. 609 (2000) 104–109;
(b) L.J. Pereira, K.S. Chan, W.K. Leong, J. Organomet. Chem. 690 (2005) 1033–1043;
(c) L.J. Pereira, W.K. Leong, J. Organomet. Chem. 691 (2006) 1941–1944;
(d) L.J. Pereira, W.K. Leong, J. Organomet. Chem. 691 (2006) 2448–2456;
(e) L.J. Pereira, W.K. Leong, Polyhedron 25 (2006) 2392–2400.

[3] (a) Y.L.K. Tan, W.K. Leong, J. Organomet. Chem. 691 (2006) 2048–2054;
(b) Y.L.K. Tan, C.W.A. Koh, T.B. Lim, W.K. Leong, J. Cluster Sci. 17 (2006) 509–516;
(c) Y.L.K. Tan, W.K. Leong, J. Organomet. Chem. 692 (2007) 768–773.

[4] P.J. Dyson, J.S. McIndoe, Transition Metal Carbonyl Cluster Chemistry, Gordon and Breach, Amsterdam, 2000.

[5] A.J. Deeming, M. Stchedroff, J. Chem. Soc., Dalton Trans. (1998) 3819–3824.

[6] (a) M.R. Churchill, R.A. Lashewycz, Inorg. Chem. 17 (1978) 1950–1957;
(b) R.D. Adams, N.M. Golembeski, J.P. Selegue, J. Am. Chem. Soc. 103 (1981) 546–555.

[7] K.A. Azam, S.E. Kabir, A. Miah, M.W. Day, K.I. Hardcastle, E. Rosenberg, A.J. Deeming, J. Organomet. Chem. 435 (1992) 157–167.

[8] (a) M. Castiglioni, R. Giordano, E. Sappa, J. Organomet. Chem. 342 (1988) 97–109;
(b) K. Natarajan, L. Zsolnai, G. Huttner, J. Organomet. Chem. 220 (1981) 365–381;
(c) W.K. Leong, Y. Liu, J. Organomet. Chem. 584 (1999) 174–178.

[9] S.P. Tunik, T.S. Pilyugina, I.O. Koshevoy, S.I. Selivanov, M. Haukka, T.A. Pakkanen, Organometallics 23 (2004) 568–579.

[10] F.H. Carré, F.A. Cotton, B.A. Frenz, Inorg. Chem. 15 (1976) 380–387.

[11] H.A. Mirza, J.J. Vittal, R.J. Puddephatt, C.S. Frampton, L. Manojlović-Muir, W. Xia, R.H. Hill, Organometallics 12 (1993) 2767–2776.

[12] N. Nawar, J. Organomet. Chem. 602 (2000) 137–143.

[13] M.I. Bruce, P.A. Humphrey, B.W. Skelton, A.H. White, J. Organomet. Chem. 526 (1996) 85–97.

[14] M. Deng, W.K. Leong, J. Chem. Soc., Dalton. Trans. (2002) 1020–1023.

[15] R.T. Morrison, R.N. Boyd, Organic Chemistry, 5th ed., Allyn & Bacon, NY, 1987.

[16] J.A. Iggo, NMR Spectroscopy in Inorganic Chemistry, OUP, Great Britain, 1999.

[17] R.F. Alex, F.W.B. Einstein, R.H. Jones, R.K. Pomeroy, Inorg. Chem. 26 (1987) 3175–3178.

[18] K-B. Shiu, S-M. Peng, M.-C. Cheng, J. Organomet. Chem. 453 (1993) 133–138.

[19] P. Homanen, R. Persson, M. Haukka, T.A. Pakkanen, E. Nordlander, Organometallics 19 (2000) 5568–5574.

[20] (a) M.J. Mays, F. Pavelčík, P.R. Raithby, P.L. Taylor, P.J. Wheatley, Acta Crystallogr., Sect. B 37 (1981) 2228–2230;
(b) K. Natarajan, L. Zsolnai, G. Huttner, J. Organomet. Chem. 220 (1981) 365–381;
(c) A.J. Deeming, S. Doherty, M.W. Day, K.I. Hardcastle, H. Minassian, J. Chem. Soc., Dalton. Trans. (1991) 1273–1279;
(d) B.F.G. Johnson, J. Lewis, E. Nordlander, P.R. Raithby, C.E. Housecroft, Inorg. Chim. Acta 259 (1997) 345–350;
(e) H.G. Ang, W.L. Kwik, W.K. Leong, B.F.G. Johnson, J. Lewis, P.R. Raithby, J. Organomet. Chem. 396 (1990) C43–C46;
(f) S.B. Colbran, P.T. Irele, B.F.G. Johnson, F.J. Lahoz, J. Lewis, P.R. Raithby, J. Chem. Soc., Dalton Trans. (1989) 2023–2031;
(g) F. Iwasaki, M.J. Mays, P.R. Raithby, P.L. Taylor, P.J. Wheatley, J. Organomet. Chem. 213 (1981) 185–206.

[21] (a) M.P. Felicissimo, A.A. Batista, A.G. Ferreira, J. Ellena, E.E. Castellano, Polyhedron 24 (2005) 1063–1070;
(b) W. Fan, R. Zhang, W.K. Leong, Y.K. Yan, Inorg. Chim. Acta 357 (2004) 2441–2450;
(c) J. Ruiz, M.E.G. Mosquera, V. Riera, J. Organomet. Chem. 527 (1997) 35–41;

(d) R.W. Hilts, S.J. Sherlock, M. Cowie, E. Singleton, M.M. de V. Steyn, Inorg. Chem. 29 (1990) 3161–3167.
[22] (a) H. Adams, M.T. Atkinson, M.J. Morris, J. Organomet. Chem. 633 (2001) 125–130;
(b) H. Song, K. Lee, J.T. Park, H.Y. Chang, M.G. Choi, J. Organomet. Chem. 599 (2000) 49–56;
(c) D.N. Horng, C.H.J. Ueng, J. Organomet. Chem. 505 (1995) 53–61;
(d) D.J. Blumer, K.W. Barnett, T.L. Brown, J. Organomet. Chem. 173 (1979) 71–76.
[23] K.S. Gan, H.K. Lee, T.S.A. Hor, J. Organomet. Chem. 460 (1993) 197–202.
[24] G.R. County, S.M. Dickson, S.M. Jenkins, J. Johnson, O. Paravagna, J. Organomet. Chem. 530 (1997) 49–57.
[25] W. Fan, R. Zhang, W.K. Leong, C.K. Chu, Y.K. Yan, J. Organomet. Chem. 690 (2005) 3765–3773.
[26] A.J. Deeming, D.M. Speel, M. Stchedroff, Organometallics 16 (1997) 6004–6009.
[27] SMART version 5.628, Bruker AXS Inc., Madison, WI, USA, 2001.
[28] SAINT+ version 6.22a, Bruker AXS Inc., Madison, WI, USA, 2001.
[29] Sheldrick, G.M. SADABS, 1996.
[30] SHELXTL version 5.1, Bruker AXS Inc., Madison, WI, USA, 1997.
[31] Orpen, A.G. XHYDEX, School of Chemistry, University of Bristol, UK, 1997.